

Supervised binary classification of small-scale digits images with a trapped-ion quantum processor

Ilia V. Zalivako,^{1,2} Alexander I. Gircha,^{1,2} Anastasiia S. Nikolaeva,^{1,2} Denis A. Drozhzhin,^{1,2} Alexander S. Borisenko,^{1,2} Andrei E. Korolkov,^{1,2} Nikita V. Semenin,^{1,2} Kristina P. Galstyan,^{1,2} Pavel A. Kamenskikh,^{1,2} Vasilii N. Smirnov,^{1,2} Mikhail A. Aksenov,² Pavel L. Sidorov,^{1,2} Evgeniy O. Kiktenko,^{1,2} Ksenia Yu. Khabarova,^{1,2} Aleksey K. Fedorov,^{1,2} Nikolay N. Kolachevsky,^{1,2} and Ilya A. Semerikov^{1,2}

¹*P.N. Lebedev Physical Institute of the Russian Academy of Sciences, Moscow 119991, Russia*

²*Russian Quantum Center, Skolkovo, Moscow 121205, Russia*

Here we present the results of benchmarking of a quantum processor based on trapped $^{171}\text{Yb}^+$ ions by performing basic quantum machine learning algorithms. Specifically, we carry out a supervised binary classification of small-scale digits images, which are intentionally chosen so that they can be classified with 100% accuracy, using a quantum-enhanced Support Vector Machine algorithm with up to four qubits. In our work, we specifically consider different types of quantum encodings of the dataset and different levels of transpilation optimizations for the corresponding quantum circuits. For each quantum encoding, we obtain a classifier that is of 100% accuracy on both training and test sets, which demonstrates that the quantum processor can correctly solve the basic classification task considered. As we expect, with the increase of the capabilities quantum processors, they can become a useful tool for machine learning.

I. INTRODUCTION

Recent progress in developing quantum computing devices has shown their potential to solve computational problems at the threshold of capabilities of computing devices based on classical principles [1–4]. Various physical platforms for quantum computing, such as superconducting circuits [1, 5], semiconductor quantum dots [6–8], photonic systems [2, 9], neutral atoms [10–13], and trapped ions [14–16], are currently under development. Although such quantum devices are used to solve certain classes of computational problems [10–16], demonstration of a sizable computational advantage in solving practical problems remains a challenge [17]. This quest for practical quantum computational advantage poses interesting problems. On the one hand, one needs to increase the computational capabilities of quantum computers, which requires not only scaling to the significant number of qubits but also improving the quality of quantum operations (i.e., quantum gate fidelities). From this point of view, trapped-ion-based quantum processors demonstrate the highest quantum volume of 2^{20} in experiments by Quantinuum [18]. In addition, trapped-ion-based quantum devices have been used to demonstrate error correction [19–24], e.g., a fault-tolerant entanglement between two logical qubits [24, 25] and quantum algorithms with logical qubits [26] have been realized. Therefore, such systems seem to be promising for running quantum algorithms [17, 27, 28].

On the other hand, a problem to solve on a quantum processor should be chosen carefully. Candidates include integer factorization [29] and simulating complex quantum systems [30]. However, achieving quantum advantage in these directions seems to require computational resources that are far beyond the capabilities of the upcoming generation of quantum devices [17]. One of the directions, which is under exploration in the con-



FIG. 1. Training and test datasets of digits images. All images are naturally divided into two classes, depicting zeroes and ones, respectively.

text of near-term applications, is the field of quantum machine learning [31]. Various approaches have been proposed. In particular, quantum convolutional neural networks [32–34], generative adversarial networks [35–37], kernel methods [38–40], and other approaches have been studied. Recent experimental works in the field of quantum machine learning [41] include classifiers for handwritten digits datasets [42–44], analyzing NMR readings [45, 46], classification of lung cancer patients [47], classifying and ranking DNA to RNA transcription factors [48], satellite imagery analysis [49], generative chemistry [50] weather forecasting [51], and many others (for a review, see Refs. [31, 52, 53]). Therefore, benchmarking quantum processors under development using quantum machine learning tasks seems to be useful as a step towards demonstrating quantum computational advantage for practically-relevant problems.

Here we present the results of benchmarking of a quantum processor based on trapped $^{171}\text{Yb}^+$ ions by implementing a quantum machine learning algorithm with the use of up to four qubits. We perform a supervised binary classification of small-scale digits images from a publicly available dataset, shown in Fig. 1, using a quantum-enhanced support vector machine (SVM) algorithm [39, 40]. The images are intentionally chosen so

that they can be classified with 100% accuracy. We consider different types of quantum encodings of the dataset and several degrees of transpilation optimizations for corresponding quantum circuits. For each quantum encoding, we obtain a classifier that is 100% accurate on both training and test sets. Our results demonstrate that the quantum processor can correctly solve the basic, small-scale classification task considered; as we expect, with the increase of their capabilities quantum processors have the potential to become a useful tool for machine learning applications.

II. QUANTUM-ENHANCED SVM

In this section, we briefly revisit the fundamental concepts underlying the binary classification using the quantum-enhanced SVM. For more detailed information, we refer the reader to Refs. [39, 40]. Let $\{(\mathbf{x}_i, l_i)\}_{i=1}^L$ denote an L -element labeled training dataset, consisting of feature vectors $\mathbf{x}_i \in \mathbb{R}^d$, where d is the dimensionality of the feature space, and corresponding labels $l_i = \pm 1$. Within the standard SVM framework, predicting a label l' for a test sample \mathbf{x}' can be formulated as:

$$\begin{aligned} l' &:= \text{sign}(K(\mathbf{x}', \mathbf{w}) + b) \\ &= \text{sign}\left(\sum_{s \in S} \alpha_s l_s K(\mathbf{x}', \mathbf{x}_s) + b\right) \end{aligned} \quad (1)$$

with $\mathbf{w} = \sum_{s \in S} \alpha_s l_s \mathbf{x}_s$. Here $K(\cdot, \cdot) : \mathbb{R}^d \times \mathbb{R}^d \rightarrow \mathbb{R}$ represents a *kernel function*, which is a prespecified function that provides positive semidefiniteness property to every matrix $(K(\mathbf{y}_i, \mathbf{y}_j))_{ij}$ constructed based on an arbitrary finite set of feature vectors $\{\mathbf{y}_i\}$; the subset $S \subset \{1, \dots, L\}$ is a collection of indices of *support vectors* taken from the training dataset; and α_s, b are real numbers. The values of $S, \{\alpha_s\}$, and b come from the training process. More specifically, $\{\alpha_i\}_{i=1}^L$ appears as the solution to the quadratic programming optimization problem

$$\begin{aligned} \frac{1}{2} \sum_{i,j=1}^L \alpha_i \alpha_j l_i l_j K(\mathbf{x}_i, \mathbf{x}_j) - \sum_{i=1}^L \alpha_i &\rightarrow \min \quad \text{s.t.} \\ 0 \leq \alpha_i \leq C \text{ for } i = 1, \dots, L, \quad \sum_{i=1}^L \alpha_i l_i &= 0, \end{aligned} \quad (2)$$

where $C > 0$ is a regularization parameter; the set of support vectors indices S is defined as a subset of $i \in \{1, \dots, L\}$ with $\alpha_i > 0$; and

$$b := \frac{1}{|S|} \sum_{s \in S} \left(l_s - \sum_{m \in S} \alpha_m l_m K(\mathbf{x}_m, \mathbf{x}_s) \right), \quad (3)$$

where $|S|$ is the number of elements in S . Intuitively, as a result of the training process, the entire space of feature vectors $\mathbf{x} \in \mathbb{R}^d$ is divided into two regions:

$$K(\mathbf{x}, \mathbf{w}) + b \geq 0 \quad \text{and} \quad K(\mathbf{x}, \mathbf{w}) + b < 0, \quad (4)$$

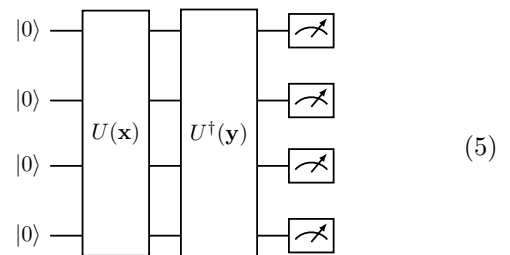
corresponding to labels of $+1$ and -1 , respectively. The border of the division is specified by \mathbf{w} and b that are determined by a limited set of support vectors with their labels $\{(\mathbf{x}_s, l_s)\}_{s \in S}$ and coefficients $\{\alpha_s\}_{s \in S}$. The crucial fact is that the optimization problem (2) can be efficiently solved using standard quadratic optimization methods in polynomial time, provided that the elements of the *kernel matrix* $K_{ij} := K(\mathbf{x}_i, \mathbf{x}_j)$ have been precomputed.

The elements of the kernel matrix $K(\mathbf{x}, \mathbf{y})$ can be interpreted as an inner product $\phi(\mathbf{x}) \cdot \phi(\mathbf{y})$ of some vectors $\phi(\mathbf{x})$ and $\phi(\mathbf{y})$. These vectors may have a dimension that is significantly different from the original feature space. During the training process, defined by Eq. (2) and Eq. (3), and prediction described by Eq. (1), only scalar products of the form $K(\mathbf{x}_i, \mathbf{x}_j)$ and $K(\mathbf{x}_s, \mathbf{x}')$ are required (there is no need to explicitly compute the $\phi(\cdot)$ vectors). The concept of quantum-enhanced SVM is based on the design of a kernel function, $K(\cdot, \cdot)$, that can be calculated on a quantum computer. This kernel function corresponds to the embedding of the original feature vectors into a Hilbert space of quantum states. In this scenario, the mapping from feature vectors to their corresponding quantum states may take on a quite complex form due to the creation of entangled quantum states during the calculation of individual kernel elements. In the next section a specific implementation of the considered quantum-enhanced SVM algorithm is provided.

III. SUPERVISED CLASSIFICATION OF DIGITS IMAGES

Here we consider a task of digits images supervised binary classification with the use of the quantum-enhanced SVM approach. In particular, we consider a small subset of images of handwritten digits zero and one from the Optdigits dataset [54]. Training and test datasets of digits images are shown in Fig. 1. The training set contains 6 images, the test set contains 4 images. All images are naturally divided into two classes, depicting zeros and ones, respectively. The size of each image is 8×8 pixels.

The process of the kernel matrix estimation is performed with the following quantum circuit:



Here $U(\mathbf{x})$ stands for an embedding circuit, transforming an initial state $|0\rangle^{\otimes N}$ into a state $|\phi(\mathbf{x})\rangle$, corresponding to the image \mathbf{x} . Here N denotes the number of used

qubits. It is followed by the action of $U^\dagger(\mathbf{y})$ and terminated by the measurement. The kernel matrix element

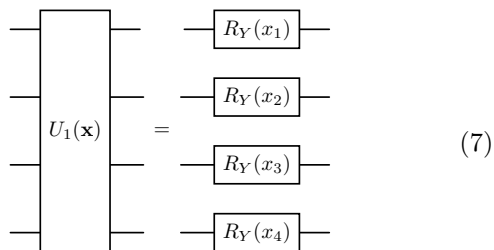
$$K(\mathbf{x}, \mathbf{y}) = |\langle \phi(\mathbf{x}) | \phi(\mathbf{y}) \rangle|^2, \quad (6)$$

which is the fidelity between states $|\phi(\mathbf{x})\rangle$ and $|\phi(\mathbf{y})\rangle$, is then given by the probability of finding the quantum register back in the state $|0\rangle^{\otimes N}$.

To allow SVM algorithm to build 100% accurate classifier, the encoding circuit should be chosen in such a way, that embedded points of different classes (images of zeros and ones) are linearly separable. That is, there must be some hyperplane in the Hilbert space which separates all points from the one class from another. In this work we consider three encoding methods.

As the first preprocessing step for all three encodings, we scale pixel intensities of all considered digits images to values between 0 and 1. For simplicity, we use only the central pixels of the digits images as they provide enough information for classification. For the first two encodings, we select from each image the intensities of pixels with coordinates (3, 3), (3, 4), (4, 3) and (4, 4), multiply them by π and flatten them as a vector $\mathbf{x} = (x_1, x_2, x_3, x_4)$.

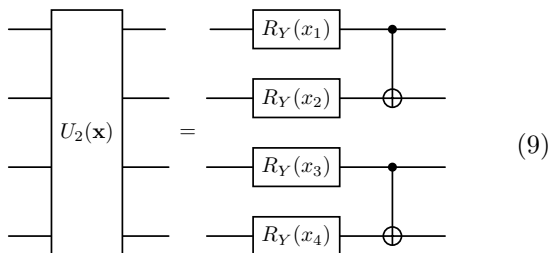
The first and the simplest encoding consists of a layer of R_Y gates on 4 qubits, where R_Y stands for a standard rotation around Y -axis on the Bloch sphere:



The kernel matrix elements for this encoding in the absence of noise are given by the relation

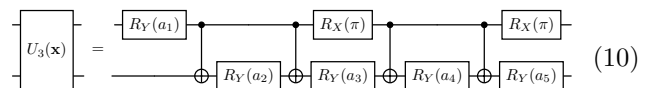
$$K(\mathbf{x}, \mathbf{y}) = \prod_{i=1}^4 \cos\left(\frac{x_i - y_i}{2}\right)^2. \quad (8)$$

In the second encoding, in order to study effect of the two-qubit gates noise on the classification accuracy, we add another layer of two controlled-NOT CX gates:



Kernel matrix elements in this case in the noiseless case should be the same as for the first encoding method and are given by Eq. (8).

The third embedding relies on the amplitude encoding approach [55, 56]. Its idea is to prepare a quantum state with amplitudes that are equal to the components of a given unit Euclidean vector $\bar{\mathbf{x}}$. An advantage of such embedding is that due to usage of entanglement it allows one to encode more information in the same number of qubits. Namely, a unit vector with 2^N components can be encoded using N qubits. Here we use $N = 2$ qubits to encode values of three central pixels with coordinates (3, 3), (3, 4), and (4, 4). Their intensities scaled to values between 0 and 1 and padded with 0.25 form a vector $\mathbf{x} = (x_1, x_2, x_3, 0.25)$. As amplitude encoding can be applied only to unit vectors, we normalize it: $\bar{\mathbf{x}} = \mathbf{x}/|\mathbf{x}|$. The padding prevents the case where all components of \mathbf{x} are zero and normalization is impossible. Afterwards we calculate rotation angles $\mathbf{a} = (a_1, a_2, a_3, a_4, a_5)$ for the gates in the following amplitude encoding circuit:



Rotation angles \mathbf{a} are calculated as follows [57]:

$$\begin{aligned} \mathbf{a} &:= (\beta_2, -\beta_1/2, \beta_1/2, -\beta_0/2, \beta_0/2), \\ \beta_0 &:= 2 \arcsin(\bar{x}_2 / \sqrt{\bar{x}_1^2 + \bar{x}_2^2 + \varepsilon}), \\ \beta_1 &:= 2 \arcsin(\bar{x}_4 / \sqrt{\bar{x}_3^2 + \bar{x}_4^2 + \varepsilon}), \\ \beta_2 &:= 2 \arcsin(\bar{x}_3^2 + \bar{x}_4^2). \end{aligned} \quad (11)$$

Here, vector $\bar{\mathbf{x}} = (\bar{x}_1, \bar{x}_2, \bar{x}_3, \bar{x}_4)$ is a result of the \mathbf{x} normalization and $\varepsilon = 10^{-12}$ is used to prevent division by zero. We note that circuit 10 and formulas 11 are valid only when all components of $\bar{\mathbf{x}}$ are non-negative, which is the case here. From the circuit, given by expression (10), it can be seen that the cost of more dense information encoding is increased number of two-qubit operations, which usually are the most noisy elements in all quantum algorithms. The kernel matrix in the absence of noise here is given by

$$K(\mathbf{x}, \mathbf{y}) = |\langle \bar{\mathbf{x}} | \bar{\mathbf{y}} \rangle|^2. \quad (12)$$

In what follows, we refer to these encodings as (i) R_Y , (ii) $R_Y + CX$, and (iii) amplitude encodings, correspondingly. Analytically, all three encodings send vectors \mathbf{x} , which correspond to various classes, to different areas in the quantum state space, thus making the images of each embedding linearly separable and allowing one to use the SVM algorithm for constructing 100% accurate separating hyperplane in each case.

We employ the classical implementation of the SVM algorithm from the Scikit-learn toolkit [58]. We use default values of the parameters of the algorithm, in particular, regularization parameter $C = 1$. 100% accuracy on both training and test sets in the experiments using a quantum emulator for each quantum encoding is obtained. In what follows, we describe the experiments that have been performed using the trapped-ion quantum processor.

IV. TRAPPED-ION QUANTUM PROCESSOR

Ytterbium ($^{171}\text{Yb}^+$) ions are actively used in quantum technologies, specifically, metrology [59–61] and computing [62–65]. This species possesses a convenient energy structure, which allows one to use its efficient and ensure relatively simple laser cooling [66], state initialization and readout [67, 68]. Rich level structure also provides several ways of qubits encoding, such as in hyperfine sublevels of the ground state $^2S_{1/2}$ (microwave qubit) [69–71] or in the states coupled by a narrow E2 optical transition $^2S_{1/2} \rightarrow ^2D_{3/2}$ (optical qubit) [65].

Our quantum processor (its detailed description can be found in Ref. [65]) is based on a string of 10 $^{171}\text{Yb}^+$ ions inside a linear Paul trap. The trap secular frequencies are $\{\omega_x, \omega_y, \omega_z\} = 2\pi \times \{3.650, 3.728, 0.129\}$ MHz. The qubits are encoded in states $|0\rangle = ^2S_{1/2}(F=0, m_F=0)$ and $|1\rangle = ^2D_{3/2}(F=2, m_F=0)$ coupled by an optical transition at 435.5 nm with an upper state lifetime of $\tau = 53$ ms. Our processor also supports the qudit regime [65, 72], where other Zeeman sublevels of the upper state are used for information encoding as well. Although qudit encoding may provide various advantages, in particular, for decompositions of multiqubit gates [73–78], below we focus on the qubit regime with states $|0\rangle$ and $|1\rangle$.

Before each experimental shot, the ion chain is cooled to the ground state along trap axes x and y , and all ions are initialized to the $|0\rangle$ state by optical pumping. After that, quantum gates are applied to the qubits. Quantum gates are performed by applying laser pulses at 435.5 nm to the ions. For this purpose, the setup is equipped with two addressing beams, which can be scanned along the ion chain using acousto-optical deflectors and individually interact with particular qubits.

As single-qubit gates the system supports

$$R_\phi(\theta) = \exp(-i\sigma_\phi\theta/2), \quad (13)$$

where $\sigma_\phi = \sigma_x \cos \phi + \sigma_y \sin \phi$, σ_x and σ_y are standard Pauli matrices, and ϕ, θ are arbitrary real angles. The fidelity of such operation is 99.4%, measured using randomized benchmarking. As a two-qubit gate, we use maximally entangling Mølmer-Sørensen gate [79–82] gate

$$\text{MS}(\pi/4) = \exp\left(-i\frac{\pi}{4}\sigma_x \otimes \sigma_x\right). \quad (14)$$

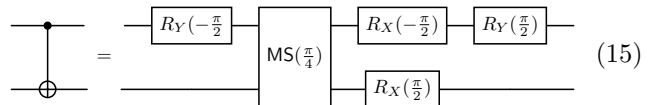
It’s fidelity was measured to be 92.7% by measuring parity oscillations after Bell state preparation.

The gates sequence is followed by the readout procedure implemented using electron shelving technique [68, 83] with a mean error of approximately 1% per ion.

As it can be seen from expressions 5, 7, 9, and 10, our circuits contain only single-qubit rotations, which are included in the native gate set, and CX gates. In the first case of non-optimized transpilation we just replace all CX gates in circuits with the following decomposition:

		Non-optimized transpilation		Optimized transpilation	
Enc.	Shots	Training	Test	Training	Test
R_Y	2048	100 (0.09)	100 (0.08)	-	-
	2048	100 (0.06)	100 (0.06)	-	-
	2048	100 (0.07)	100 (0.05)	-	-
$R_Y + \text{CX}$	1024	100 (0.32)	100 (0.32)	100 (0.08)	100 (0.09)
	1024	100 (0.52)	100 (0.35)	100 (0.04)	100 (0.05)
	1024	100 (0.24)	100 (0.24)	100 (0.06)	100 (0.02)
Ampl.	1024	100 (0.45)	100 (0.48)	100 (0.44)	100 (0.6)
	1024	83 (0.53)	100 (0.6)	100 (0.5)	100 (0.43)

TABLE I. Accuracy of each classifier in percentages (in brackets, distance to the ideal case, see below) that were obtained in all experiments on training and test datasets with all encodings for both optimized and non-optimized transpilation. The distance is defined as $d(A, B) = \max_{ij} |A_{ij} - B_{ij}|$, where A and B are kernel matrices measured using the quantum processor and quantum emulator.



Here $R_X(\theta) := R_0(\theta)$ and $R_Y(\theta) := R_{\pi/2}(\theta)$.

We also have studied algorithm performance and robustness with another transpilation scheme, which we further refer to as “optimized transpilation”. In this case we take the transpiled circuits we described above and apply the following optimizations: (i) combine several single-qubit rotations around the same axis into one rotation; (ii) eliminate single-qubit rotations where, after combining, rotation angle is a multiply of 2π ; (iii) eliminate two consecutive CX gates. Such actions significantly reduce number of both single- and two-qubit operations and, therefore, noise level.

V. RESULTS

We summarize the experimental results in the table I. For a more detailed characterization of the results, we also added in Table I distances between kernel matrices, obtained experimentally and calculated with an ideal emulator. Here we define distance as $d(A, B) = \max_{ij} |A_{ij} - B_{ij}|$, where A and B are matrices to compare.

For the first R_Y encoding, we performed three separate experiments on the same dataset and trained three classifiers. As difference between optimized and non-optimized transpilation here is negligible, we performed these experiments only for non-optimized circuits. In each experiment, 2048 shots were made for every circuit. The accuracy of each classifier was obtained to be equal to 100% on both training and test sets.

For the second $R_Y(\theta)+CX$ encoding, we ran the experiment three times for both optimized and non-optimized transpilation. In total, we have performed six experiments on the same dataset and trained six classifiers with 1024 shots used for every circuit in each experiment. As for the first R_Y encoding, the accuracy of each classifier was 100% in all cases.

For amplitude encoding, we ran the experiment two times for both optimized and non-optimized transpilation. In this case, 1024 shots for each circuit were performed. In total, four experiments on the same dataset and training of four classifiers have been performed. Among executed quantum circuits, this encoding is the most hardware-demanding as each circuit consists in non-optimized case of 8 two-qubit gates. Therefore, due to the noise, the achieved accuracy of one classifier on the training set appeared to be 83%. However, in all other experiments with amplitude encoding, the achieved accuracy of each classifier is 100%.

VI. DISCUSSION

The main target parameter in our task is the classification accuracy on both training and test datasets. The fact that in all our experiments we achieve 100% classification accuracy proves sufficient the robustness of the algorithm to the quantum processor's noise as well as sufficient quality and stability of the processor's quantum gates.

To further investigate how noise in considered encoding circuits with different circuit structures and their optimization modes affects the kernel matrix estimation procedure, we analyze the calculated average distances between experimentally obtained kernel matrices and ones calculated using a noiseless emulator (values in brackets in table I). In the ideal case, when there is no noise in a real quantum processor, the distances should be equal to zero. From Table I one can see that the distance grows

with the number of two-particle gates in the circuits, in both optimized and non-optimized transpilation modes. Since two-particle gates contribute the most to the total error, this is an expected behavior.

On the other hand, optimized transpilation also significantly reduces the error and the distance between kernel matrices. A clear example is optimized transpilation for $R_Y + CX$ encoding, where all two-particle gates are eliminated and distance is significantly decreased compared to non-optimized transpilation mode. We note that for amplitude encoding, where the number of two-particle gates cannot be reduced as much as in $R_Y + CX$ encoding, the distance between kernel matrices remains almost the same for both transpilation modes.

VII. CONCLUSION

We have performed a proof-of-principle quantum machine learning experiment using the developed trapped-ion-based quantum processor. We have considered three different quantum encodings of the dataset and compared results for both optimized and non-optimized transpilation modes. We have shown that in our experiments, despite the error in the kernel matrices estimation procedure increases with the raising of the two-qubit gates number in the circuits, the final result accuracy (classification accuracy) remains stable. For each encoding, we have developed the classifier working with 100% accuracy on both training and test sets. Our results indicate the ability of the quantum processor to correctly solve basic, small-scale classification tasks considered. As we expect, with the increase in capabilities, quantum computing devices have a potential to become a useful tool for machine learning applications.

ACKNOWLEDGEMENTS

This work was supported by the Russian Roadmap on Quantum Computing (Contract No. 868-1.3-15/15-2021, October 5, 2021).

[1] F. Arute, K. Arya, R. Babbush, D. Bacon, J. C. Bardin, R. Barends, R. Biswas, S. Boixo, F. G. S. L. Brandao, D. A. Buell, B. Burkett, Y. Chen, Z. Chen, B. Chiaro, R. Collins, W. Courtney, A. Dunsworth, E. Farhi, B. Foxen, A. Fowler, C. Gidney, M. Giustina, R. Graff, K. Guerin, S. Habegger, M. P. Harrigan, M. J. Hartmann, A. Ho, M. Hoffmann, T. Huang, T. S. Humble, S. V. Isakov, E. Jeffrey, Z. Jiang, D. Kafri, K. Kechedzhi, J. Kelly, P. V. Klimov, S. Knysh, A. Korotkov, F. Kostritsa, D. Landhuis, M. Lindmark, E. Lucero, D. Lyakh, S. Mandrà, J. R. McClean, M. McEwen, A. Megrant, X. Mi, K. Michielsen, M. Mohseni, J. Mutus, O. Naaman, M. Neeley, C. Neill, M. Y. Niu, E. Ostby, A. Petukhov, J. C. Platt, C. Quintana, E. G. Rieffel, P. Roushan, N. C. Rubin, D. Sank,

K. J. Satzinger, V. Smelyanskiy, K. J. Sung, M. D. Trevithick, A. Vainsencher, B. Villalonga, T. White, Z. J. Yao, P. Yeh, A. Zalcman, H. Neven, and J. M. Martinis, Quantum supremacy using a programmable superconducting processor, *Nature* **574**, 505 (2019).
 [2] H.-S. Zhong, H. Wang, Y.-H. Deng, M.-C. Chen, L.-C. Peng, Y.-H. Luo, J. Qin, D. Wu, X. Ding, Y. Hu, P. Hu, X.-Y. Yang, W.-J. Zhang, H. Li, Y. Li, X. Jiang, L. Gan, G. Yang, L. You, Z. Wang, L. Li, N.-L. Liu, C.-Y. Lu, and J.-W. Pan, Quantum computational advantage using photons, *Science* **370**, 1460 (2020).
 [3] H.-S. Zhong, Y.-H. Deng, J. Qin, H. Wang, M.-C. Chen, L.-C. Peng, Y.-H. Luo, D. Wu, S.-Q. Gong, H. Su, Y. Hu, P. Hu, X.-Y. Yang, W.-J. Zhang, H. Li, Y. Li, X. Jiang, L. Gan, G. Yang, L. You, Z. Wang, L. Li, N.-L. Liu, J. J.

- Renema, C.-Y. Lu, and J.-W. Pan, Phase-programmable gaussian boson sampling using stimulated squeezed light, *Phys. Rev. Lett.* **127**, 180502 (2021).
- [4] S. Ebadi, A. Keesling, M. Cain, T. T. Wang, H. Levine, D. Bluvstein, G. Semeghini, A. Omran, J.-G. Liu, R. Samajdar, X.-Z. Luo, B. Nash, X. Gao, B. Barak, E. Farhi, S. Sachdev, N. Gemelke, L. Zhou, S. Choi, H. Pichler, S.-T. Wang, M. Greiner, V. Vuletić, and M. D. Lukin, Quantum optimization of maximum independent set using rydberg atom arrays, *Science* **376**, 1209 (2022).
- [5] Y. Wu, W.-S. Bao, S. Cao, F. Chen, M.-C. Chen, X. Chen, T.-H. Chung, H. Deng, Y. Du, D. Fan, M. Gong, C. Guo, C. Guo, S. Guo, L. Han, L. Hong, H.-L. Huang, Y.-H. Huo, L. Li, N. Li, S. Li, Y. Li, F. Liang, C. Lin, J. Lin, H. Qian, D. Qiao, H. Rong, H. Su, L. Sun, L. Wang, S. Wang, D. Wu, Y. Xu, K. Yan, W. Yang, Y. Yang, Y. Ye, J. Yin, C. Ying, J. Yu, C. Zha, C. Zhang, H. Zhang, K. Zhang, Y. Zhang, H. Zhao, Y. Zhao, L. Zhou, Q. Zhu, C.-Y. Lu, C.-Z. Peng, X. Zhu, and J.-W. Pan, Strong quantum computational advantage using a superconducting quantum processor, *Phys. Rev. Lett.* **127**, 180501 (2021).
- [6] X. Xue, M. Russ, N. Samkharadze, B. Undseth, A. Sammak, G. Scappucci, and L. M. K. Vandersypen, Quantum logic with spin qubits crossing the surface code threshold, *Nature* **601**, 343 (2022).
- [7] M. T. Madzik, S. Asaad, A. Youssry, B. Joecker, K. M. Rudinger, E. Nielsen, K. C. Young, T. J. Proctor, A. D. Baczewski, A. Laucht, V. Schmitt, F. E. Hudson, K. M. Itoh, A. M. Jakob, B. C. Johnson, D. N. Jamieson, A. S. Dzurak, C. Ferrie, R. Blume-Kohout, and A. Morello, Precision tomography of a three-qubit donor quantum processor in silicon, *Nature* **601**, 348 (2022).
- [8] A. Noiri, K. Takeda, T. Nakajima, T. Kobayashi, A. Sammak, G. Scappucci, and S. Tarucha, Fast universal quantum gate above the fault-tolerance threshold in silicon, *Nature* **601**, 338 (2022).
- [9] L. S. Madsen, F. Laudenbach, M. F. Askarani, F. Rortais, T. Vincent, J. F. F. Bulmer, F. M. Miatto, L. Neuhaus, L. G. Helt, M. J. Collins, A. E. Lita, T. Gerrits, S. W. Nam, V. D. Vaidya, M. Menotti, I. Dhand, Z. Vernon, N. Quesada, and J. Lavoie, Quantum computational advantage with a programmable photonic processor, *Nature* **606**, 75 (2022).
- [10] S. Ebadi, T. T. Wang, H. Levine, A. Keesling, G. Semeghini, A. Omran, D. Bluvstein, R. Samajdar, H. Pichler, W. W. Ho, S. Choi, S. Sachdev, M. Greiner, V. Vuletić, and M. D. Lukin, Quantum phases of matter on a 256-atom programmable quantum simulator, *Nature* **595**, 227 (2021).
- [11] P. Scholl, M. Schuler, H. J. Williams, A. A. Eberharter, D. Barredo, K.-N. Schymik, V. Lienhard, L.-P. Henry, T. C. Lang, T. Lahaye, A. M. Läuchli, and A. Browaeys, Quantum simulation of 2d antiferromagnets with hundreds of rydberg atoms, *Nature* **595**, 233 (2021).
- [12] L. Henriot, L. Beguin, A. Signoles, T. Lahaye, A. Browaeys, G.-O. Reymond, and C. Jurczak, Quantum computing with neutral atoms, *Quantum* **4**, 327 (2020).
- [13] T. M. Graham, Y. Song, J. Scott, C. Poole, L. Phuttitarn, K. Jooya, P. Eichler, X. Jiang, A. Marra, B. Grinkemeyer, M. Kwon, M. Ebert, J. Cherek, M. T. Lichtman, M. Gillette, J. Gilbert, D. Bowman, T. Ballance, C. Campbell, E. D. Dahl, O. Crawford, N. S. Blunt, B. Rogers, T. Noel, and M. Saffman, Multi-qubit entanglement and algorithms on a neutral-atom quantum computer, *Nature* **604**, 457 (2022).
- [14] J. Zhang, G. Pagano, P. W. Hess, A. Kyprianidis, P. Becker, H. Kaplan, A. V. Gorshkov, Z. X. Gong, and C. Monroe, Observation of a many-body dynamical phase transition with a 53-qubit quantum simulator, *Nature* **551**, 601 (2017).
- [15] R. Blatt and C. F. Roos, Quantum simulations with trapped ions, *Nature Physics* **8**, 277 (2012).
- [16] C. Hempel, C. Maier, J. Romero, J. McClean, T. Monz, H. Shen, P. Jurcevic, B. P. Lanyon, P. Love, R. Babbush, A. Aspuru-Guzik, R. Blatt, and C. F. Roos, Quantum chemistry calculations on a trapped-ion quantum simulator, *Phys. Rev. X* **8**, 031022 (2018).
- [17] A. K. Fedorov, N. Gisin, S. M. Belousov, and A. I. Lvovsky, *Quantum computing at the quantum advantage threshold: a down-to-business review* (2022).
- [18] <https://www.quantinuum.com/news/quantinuum-extends-its-significant-lead-in-quantum-computing-achieving-historic-milestones-for-hardware-fidelity-and-quantum-volume>.
- [19] J. Chiaverini, D. Leibfried, T. Schaetz, M. D. Barrett, R. B. Blakestad, J. Britton, W. M. Itano, J. D. Jost, E. Knill, C. Langer, R. Ozeri, and D. J. Wineland, Realization of quantum error correction, *Nature* **432**, 602 (2004).
- [20] P. Schindler, J. T. Barreiro, T. Monz, V. Nebendahl, D. Nigg, M. Chwalla, M. Hennrich, and R. Blatt, Experimental repetitive quantum error correction, *Science* **332**, 1059 (2011).
- [21] R. Stricker, D. Vodola, A. Erhard, L. Postler, M. Meth, M. Ringbauer, P. Schindler, T. Monz, M. Müller, and R. Blatt, Experimental deterministic correction of qubit loss, *Nature* **585**, 207 (2020).
- [22] L. Egan, D. M. Debroy, C. Noel, A. Risinger, D. Zhu, D. Biswas, M. Newman, M. Li, K. R. Brown, M. Cetina, and C. Monroe, Fault-tolerant control of an error-corrected qubit, *Nature* **598**, 281 (2021).
- [23] A. Erhard, H. Poulsen Nautrup, M. Meth, L. Postler, R. Stricker, M. Stadler, V. Negnevitsky, M. Ringbauer, P. Schindler, H. J. Briegel, R. Blatt, N. Friis, and T. Monz, Entangling logical qubits with lattice surgery, *Nature* **589**, 220 (2021).
- [24] L. Postler, S. Heußen, I. Pogorelov, M. Rispler, T. Feldker, M. Meth, C. D. Marciniak, R. Stricker, M. Ringbauer, R. Blatt, P. Schindler, M. Müller, and T. Monz, Demonstration of fault-tolerant universal quantum gate operations, *Nature* **605**, 675 (2022).
- [25] C. Ryan-Anderson, N. C. Brown, M. S. Allman, B. Arkin, G. Asa-Attuah, C. Baldwin, J. Berg, J. G. Bohnet, S. Braxton, N. Burdick, J. P. Campora, A. Chernoguzov, J. Esposito, B. Evans, D. Francois, J. P. Gaebler, T. M. Gatterman, J. Gerber, K. Gilmore, D. Gresh, A. Hall, A. Hankin, J. Hostetter, D. Lucchetti, K. Mayer, J. Myers, B. Neyenhuis, J. Santiago, J. Sedlacek, T. Skripka, A. Slattery, R. P. Stutz, J. Tait, R. Tobey, G. Vittorini, J. Walker, and D. Hayes, *Implementing fault-tolerant entangling gates on the five-qubit code and the color code* (2022).
- [26] K. Yamamoto, S. Duffield, Y. Kikuchi, and D. M. Ramo, Demonstrating bayesian quantum phase estimation with quantum error detection (2023), [arXiv:2306.16608](https://arxiv.org/abs/2306.16608) [quant-ph].

- [27] S. Debnath, N. M. Linke, C. Figgatt, K. A. Landsman, K. Wright, and C. Monroe, Demonstration of a small programmable quantum computer with atomic qubits, *Nature* **536**, 63 (2016).
- [28] T. Monz, D. Nigg, E. A. Martinez, M. F. Brandl, P. Schindler, R. Rines, S. X. Wang, I. L. Chuang, and R. Blatt, Realization of a scalable shor algorithm, *Science* **351**, 1068 (2016).
- [29] P. Shor, Algorithms for quantum computation: discrete logarithms and factoring, in *Proceedings 35th Annual Symposium on Foundations of Computer Science* (1994) pp. 124–134.
- [30] S. Lloyd, Universal quantum simulators, *Science* **273**, 1073 (1996).
- [31] J. Biamonte, P. Wittek, N. Pancotti, P. Rebentrost, N. Wiebe, and S. Lloyd, Quantum machine learning, *Nature* **549**, 195 (2017).
- [32] M. Henderson, S. Shakya, S. Pradhan, and T. Cook, Quantum convolutional neural networks: powering image recognition with quantum circuits, *Quantum Machine Intelligence* **2**, 2 (2020).
- [33] I. Cong, S. Choi, and M. D. Lukin, Quantum convolutional neural networks, *Nature Physics* **15**, 1273 (2019).
- [34] D. Bokhan, A. S. Masiukova, A. S. Boev, D. N. Trubnikov, and A. K. Fedorov, Multiclass classification using quantum convolutional neural networks with hybrid quantum-classical learning, *Frontiers in Physics* **10**, 10.3389/fphy.2022.1069985 (2022).
- [35] S. Lloyd and C. Weedbrook, Quantum generative adversarial learning, *Phys. Rev. Lett.* **121**, 040502 (2018).
- [36] P.-L. Dallaire-Demers and N. Killoran, Quantum generative adversarial networks, *Phys. Rev. A* **98**, 012324 (2018).
- [37] C. Zoufal, A. Lucchi, and S. Woerner, Quantum generative adversarial networks for learning and loading random distributions, *npj Quantum Information* **5**, 103 (2019).
- [38] T. Y. Rupak Chatterjee, Generalized coherent states, reproducing kernels, and quantum support vector machines, *Quantum Information and Computation* **17**, 10.26421/qic17.15-16 (2017).
- [39] V. Havlíček, A. D. Córcoles, K. Temme, A. W. Harrow, A. Kandala, J. M. Chow, and J. M. Gambetta, Supervised learning with quantum-enhanced feature spaces, *Nature* **567**, 209 (2019).
- [40] M. Schuld and F. Petruccione, Quantum models as kernel methods, in *Machine Learning with Quantum Computers* (Springer International Publishing, Cham, 2021) pp. 217–245.
- [41] D. Risté, M. P. da Silva, C. A. Ryan, A. W. Cross, A. D. Córcoles, J. A. Smolin, J. M. Gambetta, J. M. Chow, and B. R. Johnson, Demonstration of quantum advantage in machine learning, *npj Quantum Information* **3**, 16 (2017).
- [42] M. Benedetti, J. Realpe-Gómez, and A. Perdomo-Ortiz, Quantum-assisted helmholtz machines: A quantum-classical deep learning framework for industrial datasets in near-term devices, *Quantum Science and Technology* **3**, 034007 (2018).
- [43] S. Johri, S. Debnath, A. Mocherla, A. Singh, A. Prakash, J. Kim, and I. Kerenidis, Nearest centroid classification on a trapped ion quantum computer (2020), [arXiv:2012.04145 \[quant-ph\]](https://arxiv.org/abs/2012.04145).
- [44] D. Bokhan, A. S. Masiukova, A. S. Boev, D. N. Trubnikov, and A. K. Fedorov, Multiclass classification using quantum convolutional neural networks with hybrid quantum-classical learning, *Frontiers in Physics* **10**, 10.3389/fphy.2022.1069985 (2022).
- [45] D. Sels, H. Dashti, S. Mora, O. Demler, and E. Demler, Quantum approximate bayesian computation for nmr model inference, *Nature Machine Intelligence* **2**, 396 (2020).
- [46] K. Seetharam, D. Biswas, C. Noel, A. Risinger, D. Zhu, O. Katz, S. Chattopadhyay, M. Cetina, C. Monroe, E. Demler, and D. Sels, Digital quantum simulation of nmr experiments (2021), [arXiv:2109.13298 \[quant-ph\]](https://arxiv.org/abs/2109.13298).
- [47] S. Jain, J. Ziauddin, P. Leonchyk, S. Yenkanchi, and J. Geraci, Quantum and classical machine learning for the classification of non-small-cell lung cancer patients, *SN Applied Sciences* **2**, 1088 (2020).
- [48] R. Y. Li, R. Di Felice, R. Rohs, and D. A. Lidar, Quantum annealing versus classical machine learning applied to a simplified computational biology problem, *npj Quantum Information* **4**, 14 (2018).
- [49] M. Henderson, J. Gallina, and M. Brett, Methods for accelerating geospatial data processing using quantum computers (2020), [arXiv:2004.03079 \[quant-ph\]](https://arxiv.org/abs/2004.03079).
- [50] A. I. Gircha, A. S. Boev, K. Avchaciov, P. O. Fedichev, and A. K. Fedorov, Hybrid quantum-classical machine learning for generative chemistry and drug design, *Scientific Reports* **13**, 8250 (2023).
- [51] G. R. Enos, M. J. Reagor, M. P. Henderson, C. Young, K. Horton, M. Birch, and C. Rigetti, Synthetic weather radar using hybrid quantum-classical machine learning (2021), [arXiv:2111.15605 \[quant-ph\]](https://arxiv.org/abs/2111.15605).
- [52] A. Perdomo-Ortiz, M. Benedetti, J. Realpe-Gómez, and R. Biswas, Opportunities and challenges for quantum-assisted machine learning in near-term quantum computers, *Quantum Science and Technology* **3**, 030502 (2018).
- [53] V. Dunjko and H. J. Briegel, Machine learning & artificial intelligence in the quantum domain: a review of recent progress, *Reports on Progress in Physics* **81**, 074001 (2018).
- [54] Opendigits dataset, <http://archive.ics.uci.edu/dataset/80/optical+recognition+of+handwritten+digits>.
- [55] M. Schuld and F. Petruccione, *Supervised Learning with Quantum Computers*, Quantum Science and Technology (Springer, 2018).
- [56] M. Möttönen, J. J. Vartiainen, V. Bergholm, and M. M. Salomaa, Transformation of quantum states using uniformly controlled rotations, *Quantum Information & Computation* **5**, 467–473 (2005).
- [57] M. Schuld, Variational classifier tutorial, https://pennylane.ai/qml/demos/tutorial_variational_classifier/.
- [58] Scikit-learn toolkit, <https://scikit-learn.org/>.
- [59] N. Huntemann, M. Okhapkin, B. Lipphardt, S. Weyers, C. Tamm, and E. Peik, High-accuracy optical clock based on the octupole transition in yb+ 171, *Physical Review Letters* **108**, 090801 (2012).
- [60] K. Khabarova, D. Kryuchkov, A. Borisenko, I. Zalivako, I. Semerikov, M. Aksenov, I. Sherstov, T. Abbasov, A. Tausenev, and N. Kolachevsky, Toward a new generation of compact transportable yb+ optical clocks, *Symmetry* **14**, 2213 (2022).
- [61] P. D. D. Schwindt, Y.-Y. Jau, H. Partner, A. Casias, A. R. Wagner, M. Moorman, R. P. Manginell, J. R. Kellogg, and J. D. Prestage, A highly

- miniaturized vacuum package for a trapped ion atomic clock, *Review of Scientific Instruments* **87**, 053112 (2016), <https://pubs.aip.org/aip/rsi/article-pdf/doi/10.1063/1.4948739/15779274/053112.1.online.pdf>.
- [62] C. D. Bruzewicz, J. Chiaverini, R. McConnell, and J. M. Sage, Trapped-ion quantum computing: Progress and challenges, *Applied Physics Reviews* **6**, 021314 (2019).
- [63] S. A. Moses, C. H. Baldwin, M. S. Allman, R. Ancona, L. Ascarrunz, C. Barnes, J. Bartolotta, B. Bjork, P. Blanchard, M. Bohn, *et al.*, A race-track trapped-ion quantum processor, *Physical Review X* **13**, 041052 (2023).
- [64] J.-S. Chen, E. Nielsen, M. Ebert, V. Inlek, K. Wright, V. Chaplin, A. Maksymov, E. Páez, A. Poudel, P. Maunz, *et al.*, Benchmarking a trapped-ion quantum computer with 29 algorithmic qubits, arXiv preprint arXiv:2308.05071 (2023).
- [65] I. V. Zalivako, A. S. Nikolaeva, A. S. Borisenko, A. E. Korolkov, P. L. Sidorov, K. P. Galstyan, N. V. Semenin, V. N. Smirnov, M. A. Aksenov, K. M. Makushin, E. O. Kiktenko, A. K. Fedorov, I. A. Semerikov, K. Y. Khabarova, and N. N. Kolachevsky, Towards multiqubit quantum processor based on a $^{171}\text{Yb}^+$ ion string: Realizing basic quantum algorithms (2024), arXiv:2402.03121 [quant-ph].
- [66] I. Zalivako, I. Semerikov, A. Borisenko, V. Smirnov, P. Vishnyakov, M. Aksenov, P. Sidorov, N. Kolachevsky, and K. Khabarova, Improved Wavelength Measurement of $2\text{S } 1/2 \rightarrow 2\text{P } 1/2$ and $2\text{D } 3/2 \rightarrow 3[3/2]1/2$ Transitions in Yb^+ , *Journal of Russian Laser Research* **40**, 375 (2019).
- [67] S. Ejtemaee, R. Thomas, and P. C. Haljan, Optimization of Yb^+ fluorescence and hyperfine-qubit detection, *Physical Review A* **82**, 1 (2010).
- [68] N. V. Semenin, A. S. Borisenko, I. V. Zalivako, I. A. Semerikov, K. Y. Khabarova, and N. N. Kolachevsky, Optimization of the readout fidelity of the quantum state of an optical qubit in the $^{171}\text{Yb}^+$ ion, *JETP Letters* **114**, 486 (2021).
- [69] P. Wang, C.-Y. Luan, M. Qiao, M. Um, J. Zhang, Y. Wang, X. Yuan, M. Gu, J. Zhang, and K. Kim, Single ion qubit with estimated coherence time exceeding one hour, *Nature communications* **12**, 1 (2021), publisher: Nature Publishing Group.
- [70] J. M. Pino, J. M. Dreiling, C. Figgatt, J. P. Gaebler, S. A. Moses, M. S. Allman, C. H. Baldwin, M. Foss-Feig, D. Hayes, K. Mayer, C. Ryan-Anderson, and B. Neyenhuis, Demonstration of the trapped-ion quantum ccd computer architecture, *Nature* **592**, 209 (2021).
- [71] K. Wright, K. M. Beck, S. Debnath, J. M. Amini, Y. Nam, N. Grzesiak, J. S. Chen, N. C. Pisenti, M. Chmielewski, C. Collins, K. M. Hudek, J. Mizrahi, J. D. Wong-Campos, S. Allen, J. Apisdorf, P. Solomon, M. Williams, A. M. Ducore, A. Blinov, S. M. Kreike-meier, V. Chaplin, M. Keesan, C. Monroe, and J. Kim, Benchmarking an 11-qubit quantum computer, *Nature Communications* **10**, 5464 (2019).
- [72] M. A. Aksenov, I. V. Zalivako, I. A. Semerikov, A. S. Borisenko, N. V. Semenin, P. L. Sidorov, A. K. Fedorov, K. Y. Khabarova, and N. N. Kolachevsky, Realizing quantum gates with optically addressable yb^+ 171 ion qudits, *Phys. Rev. A* **107**, 052612 (2023).
- [73] T. C. Ralph, K. J. Resch, and A. Gilchrist, Efficient toffoli gates using qudits, *Phys. Rev. A* **75**, 022313 (2007).
- [74] B. P. Lanyon, M. Barbieri, M. P. Almeida, T. Jennewein, T. C. Ralph, K. J. Resch, G. J. Pryde, J. L. O'Brien, A. Gilchrist, and A. G. White, Simplifying quantum logic using higher-dimensional hilbert spaces, *Nature Physics* **5**, 134 (2009).
- [75] R. Ionicioiu, T. P. Spiller, and W. J. Munro, Generalized toffoli gates using qudit catalysis, *Phys. Rev. A* **80**, 012312 (2009).
- [76] A. Fedorov, L. Steffen, M. Baur, M. P. da Silva, and A. Wallraff, Implementation of a toffoli gate with superconducting circuits, *Nature* **481**, 170 (2012).
- [77] P. Gokhale, J. M. Baker, C. Duckering, N. C. Brown, K. R. Brown, and F. T. Chong, Asymptotic improvements to quantum circuits via qutrits, in *Proceedings of the 46th International Symposium on Computer Architecture*, ISCA '19 (Association for Computing Machinery, New York, NY, USA, 2019) pp. 554–566.
- [78] A. S. Nikolaeva, E. O. Kiktenko, and A. K. Fedorov, Decomposing the generalized toffoli gate with qutrits, *Phys. Rev. A* **105**, 032621 (2022).
- [79] F. Schmidt-Kaler, H. Häffner, M. Riebe, S. Gulde, G. P. T. Lancaster, T. Deuschle, C. Becher, C. F. Roos, J. Eschner, and R. Blatt, Realization of the cirac-zoller controlled-not quantum gate, *Nature* **422**, 408 (2003).
- [80] K. Mølmer and A. Sørensen, Multiparticle entanglement of hot trapped ions, *Phys. Rev. Lett.* **82**, 1835 (1999).
- [81] A. Sørensen and K. Mølmer, Quantum computation with ions in thermal motion, *Phys. Rev. Lett.* **82**, 1971 (1999).
- [82] A. Sørensen and K. Mølmer, Entanglement and quantum computation with ions in thermal motion, *Phys. Rev. A* **62**, 022311 (2000).
- [83] D. Leibfried, R. Blatt, C. Monroe, and D. Wineland, Quantum dynamics of single trapped ions, *Review of Modern Physics* **75**, 281 (2003), ISBN: 0034-6861 1539-0756.